

Article

Tuning Lewis Acidity of Metal-Organic Frameworks via Perfluorination of Bridging Ligands: Spectroscopic, Theoretical, and Catalytic Studies

Pengfei Ji, Tasha Drake, Akiko Murakami, Pau Oliveres, Jonathan H. Skone, and Wenbin Lin

J. Am. Chem. Soc., **Just Accepted Manuscript** • Publication Date (Web): 26 Jul 2018

Downloaded from <http://pubs.acs.org> on July 26, 2018

Just Accepted

“Just Accepted” manuscripts have been peer-reviewed and accepted for publication. They are posted online prior to technical editing, formatting for publication and author proofing. The American Chemical Society provides “Just Accepted” as a service to the research community to expedite the dissemination of scientific material as soon as possible after acceptance. “Just Accepted” manuscripts appear in full in PDF format accompanied by an HTML abstract. “Just Accepted” manuscripts have been fully peer reviewed, but should not be considered the official version of record. They are citable by the Digital Object Identifier (DOI®). “Just Accepted” is an optional service offered to authors. Therefore, the “Just Accepted” Web site may not include all articles that will be published in the journal. After a manuscript is technically edited and formatted, it will be removed from the “Just Accepted” Web site and published as an ASAP article. Note that technical editing may introduce minor changes to the manuscript text and/or graphics which could affect content, and all legal disclaimers and ethical guidelines that apply to the journal pertain. ACS cannot be held responsible for errors or consequences arising from the use of information contained in these “Just Accepted” manuscripts.

Tuning Lewis Acidity of Metal-Organic Frameworks via Perfluorination of Bridging Ligands: Spectroscopic, Theoretical, and Catalytic Studies

Pengfei Ji,^{‡‡} Tasha Drake,^{‡‡} Akiko Murakami,[†] Pau Oliveres,[†] Jonathan H. Skone,^{||} and Wenbin Lin*[†]

[†]Department of Chemistry, The University of Chicago, 929 E 57th St, Chicago, IL 60637, USA

^{||}Research Computing Center, The University of Chicago, 5607 S. Drexel Ave, Chicago, IL 60637, USA

ABSTRACT: The Lewis acidity of metal-organic frameworks (MOFs) has attracted much research interest in recent years. We report here the development of two quantitative methods for determining the Lewis acidity of MOFs—based on electron paramagnetic resonance (EPR) spectroscopy of MOF-bound superoxide ($O_2^{\cdot -}$) and fluorescence spectroscopy of MOF-bound N-methylacridone (NMA)—and a simple strategy that significantly enhances MOF Lewis acidity through ligand perfluorination. Two new perfluorinated MOFs, Zr_6 -fBDC and Zr_6 -fBPDC, where H_2 fBDC is 2,3,5,6-tetrafluoro-1,4-benzenedicarboxylic acid and H_2 fBPDC is 2,2',3,3',5,5',6,6'-octafluoro-4,4'-biphenyldicarboxylic acid, were shown to be significantly more Lewis acidic than non-substituted UiO-66 and UiO-67 as well as the nitrated MOFs Zr_6 -BDC- NO_2 and Zr_6 -BPDC-(NO_2)₂. Zr_6 -fBDC was shown to be a highly active single-site solid Lewis acid catalyst for Diels-Alder and arene C-H iodination reactions. Thus, this work establishes the important role of ligand perfluorination in enhancing MOF Lewis acidity and the potential of designing highly Lewis acidic MOFs for fine chemical synthesis.

INTRODUCTION

Metal-organic frameworks (MOFs) have emerged as a novel class of single-site solid catalysts in the past few years.¹⁻¹⁶ MOFs are typically endowed with catalytic activity either through covalent incorporation of catalytically active species into the organic ligands or the inorganic nodes¹⁷⁻¹⁹ or through entrapment of metal nanoparticles,²⁰⁻²¹ enzymes²², or inorganic clusters in the channels.²³⁻²⁴ One class of MOF catalysts distinguishes itself from other catalysts by using the inorganic nodes as single-site catalytic centers. The metal centers in these MOFs feature unique electronic properties and steric environments that are not accessible to conventional homogeneous or heterogeneous catalytic species.²⁵⁻²⁷

In this context, early demonstrations of MOF catalysis took advantage of Lewis acidity of the metal-connecting points,²⁸⁻²⁹ but these MOFs are relatively unstable and do not possess high catalytic activities. The advent of highly stable MOFs based on early metals of d^0 electronic configurations³⁰⁻³¹ brought about porous solid catalysts with enhanced Lewis acidity for a number of catalytic reactions such as isomerization,³²⁻³³ hydrolysis,³⁴ and dehydration³⁵ among others.³⁶⁻³⁹

Despite recent progress,⁴⁰⁻⁴⁶ existing MOFs exhibit significantly lower Lewis acidity than homogeneous systems such as $Sc(OTf)_3$. In contrast to homogeneous systems, where Lewis acidity at the active sites can be precisely measured, no techniques are currently available to quantitatively assess Lewis acidity of MOF

catalysts due, in part, to the insolubility and structural complexity of MOFs. Although notable efforts have been made to use reaction kinetics to probe Lewis acidity, the reaction rates are convoluted with intrinsic Lewis acidity, diffusion rates of substrates/products through the MOF channels and in solution, and partition of substrates/products between MOF channels.^{32, 47-48} The objectives of this work are to develop quantitative methods to determine the Lewis acidity of MOFs and to discover effective strategies to enhance their Lewis acidity. Significant enhancement of Lewis acidity of MOFs can afford porous solid catalysts with much larger pores and channels than zeolites for fine chemical synthesis.

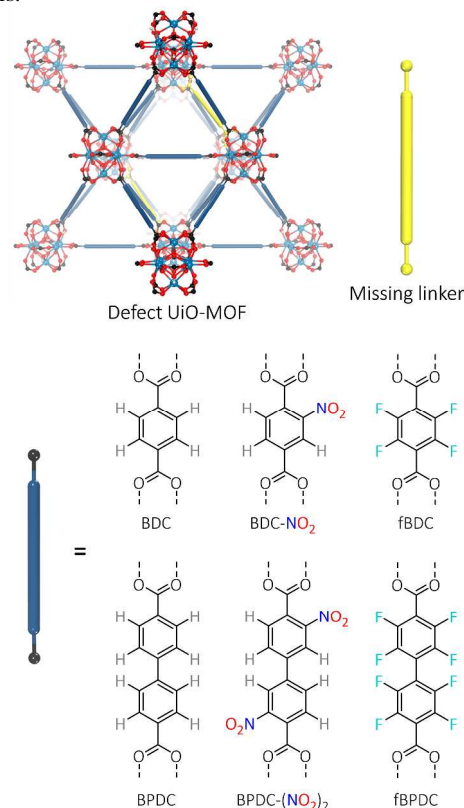


Figure 1. Framework structures and bridging ligands of two series of MOFs isostructural to UiO-66 and UiO-67 with defect $Zr_6O_4(OH)_4$ nodes studied in this work. Electron-deficient nitrated and perfluorinated bridging ligands increase Lewis acidity of Zr centers within defect nodes.

We report here the development of two general methods for determining Lewis acidity of MOFs. The first method probes Lewis acidity through the coordination of *in situ* generated superoxide which displays diagnostic electron paramagnetic resonance (EPR) features. The second method probes the Lewis acidity through the binding of a fluorescent dye with strongly coordinative electron lone pairs.⁴⁹ We prepared a series of UiO MOFs featuring defect $Zr_6O_4(OH)_4$ inorganic nodes with missing linkers and unsaturated coordination around Zr active sites.⁵⁰⁻⁵⁵ Applica-

tion of EPR and fluorescence methods to a variety of Lewis acidic MOFs, especially the MOFs with defect $Zr_6O_4(OH)_4$ nodes, has unveiled a strong correlation between dicarboxylate electron density and $Zr_6O_4(OH)_4$ Lewis acidity. Based on this insight, we have significantly enhanced the Lewis acidity of Zr-MOFs using perfluorinated bridging ligands to afford porous solid catalysts for challenging transformations typically effected by strongly Lewis acidic homogeneous catalysts (Figure 1).

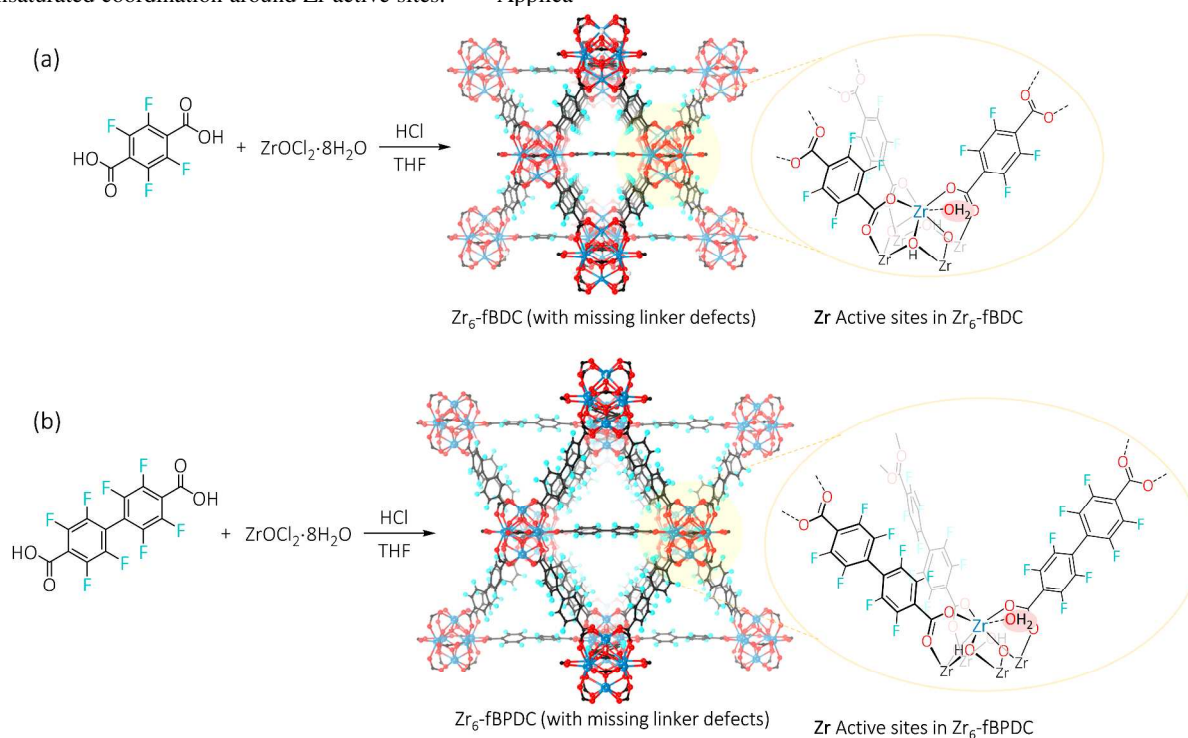


Figure 2. Synthesis of defect $Zr_6\text{-fBDC}$ (a) and $Zr_6\text{-fBPDC}$ (b) from $ZrOCl_2 \cdot 8H_2O$ and perfluorinated linkers. The missing organic linkers give rise to unsaturated coordination around the Zr_6 nodes. The coordination environments of the Zr active sites are approximately $Zr(\mu_3\text{-O})_2(\mu_3\text{-OH})_2(L)_3(OH)_2$ in these two MOFs (L is fBDC or fBPDC).

RESULTS AND DISCUSSION

Synthesis and Characterization of Perfluorinated MOFs. We have synthesized two perfluorinated UiO-MOFs, $Zr_6\text{-fBDC}$ and $Zr_6\text{-fBPDC}$, by replacing 1,4-benzenedicarboxylate (BDC) in $Zr_6\text{-BDC}$ (UiO-66) and 4,4'-biphenyldicarboxylate (BPDC) ligands in $Zr_6\text{-BPDC}$ (UiO-67) with 2,3,5,6-tetrafluoro-1,4-benzenedicarboxylate (fBDC) and 2,2',3,3',5,5',6,6'-octafluoro-4,4'-biphenyldicarboxylate (fBPDC) ligands, respectively (Figure 2). $Zr_6\text{-fBDC}$ was synthesized in 86% yield by heating a mixture of $ZrOCl_2 \cdot 8H_2O$ and $H_2\text{fBDC}$ in acidic tetrahydrofuran (THF) at 80 °C. Powder X-ray diffraction (PXRD) studies indicated that $Zr_6\text{-fBDC}$ is isostructural to UiO-66 (Figure S6, SI). The porosity of $Zr_6\text{-fBDC}$ was confirmed by N_2 sorption isotherms, which displayed a Brunauer-Emmett-Teller (BET) surface area of 1021 m^2/g . DFT fitting of the N_2 sorption isotherms of $Zr_6\text{-fBDC}$ gave pore sizes of ~6 and ~8 Å that are attributable to the tetrahedral and octahedral cages of the UiO structure, respectively (Figure S7, SI), in addition to a larger pore at ~12 Å due to the missing fBDC ligands. The surface area of $Zr_6\text{-fBDC}$ is lower than that of UiO-66 due to the increased formula weight in the perfluorinated MOF (1875 Da for $Zr_6\text{-fBDC}$ vs 1664 Da for UiO-66). Unlike previously reported perfluorinated MOFs,⁵⁶⁻⁶⁰ $Zr_6\text{-fBDC}$ features high thermal stability with a decomposition temperature of 380 °C as measured by thermal gravimetric analysis (TGA, Figure S8, SI). A combination of ^{19}F NMR and ICP-MS techniques showed the number of missing linkers to be 1.33 per Zr_6 node (Figure S5, SI). Based on this information, the formula of $Zr_6\text{-fBDC}$ is calcu-

lated to be $Zr_6(\mu_3\text{-O})_4(\mu_3\text{-OH})_4(\text{fBDC})_{4.67}[(\text{OH})(\text{OH}_2)]_{2.66}$. The defect density of $Zr_6\text{-fBDC}$ is slightly larger than that of defect UiO-66, which was reported to be 0.7 missing linkers per Zr_6 node, presumably due to the relatively weaker coordination strength of the fBDC ligand to the Zr_6 node.⁶¹ The structure of $Zr_6\text{-fBDC}$ was unaltered after desolvation and catalysis based on the retention of the $Zr_6\text{-fBDC}$ PXRD patterns.

$Zr_6\text{-fBPDC}$, a UiO-67 analogue of $Zr_6\text{-fBDC}$ with larger channels, was prepared similarly. The $H_2\text{fBPDC}$ linker was synthesized by CuCl_2 -mediated oxidative aryl-aryl coupling of the methyl tetrafluorobenzoate organozinc reagent followed by ester hydrolysis (Figure S1, SI). $Zr_6\text{-fBPDC}$ was synthesized in 90% yield by heating a mixture of $ZrOCl_2 \cdot 8H_2O$ and $H_2\text{fBPDC}$ in acidic THF at 80 °C. The PXRD pattern of $Zr_6\text{-fBPDC}$ matched well with the simulated pattern for UiO-67, indicating their isostructural nature (Figure S11, SI). Compared to $Zr_6\text{-fBDC}$, $Zr_6\text{-fBPDC}$ has a larger BET surface area of 1148 m^2/g while maintaining high thermal stability with a decomposition temperature of 310 °C as measured by TGA (Figure S12-13, SI). $Zr_6\text{-fBPDC}$ displayed two types of pores at ~12 and ~15 Å, corresponding to the tetrahedral and octahedral cages, respectively, and a larger pore at ~22 Å due to the missing fBPDC ligands. The number of missing linkers per Zr_6 node was determined by ^{19}F NMR and ICP-MS to be 1.73 per Zr_6 node, giving the formula $Zr_6(\mu_3\text{-O})_4(\mu_3\text{-OH})_4(\text{fBPDC})_{4.27}[(\text{OH})(\text{OH}_2)]_{3.46}$ for $Zr_6\text{-fBPDC}$ (Figure S10, SI).

Synthesis and Characterization of Nitrated MOFs

Zr₆-BDC-NO₂ and Zr₆-BPDC-(NO₂)₂ were synthesized to compare their Lewis acidity with those of perfluorinated MOFs. Zr₆-BDC-NO₂ was prepared from H₂BDC-NO₂ and ZrOCl₂·8H₂O in acidified DMF. PXRD studies indicated its isostructural nature with UiO-66. N₂ sorption isotherms of Zr₆-BDC-NO₂ afforded a BET surface area of 960 m²/g and pore diameters of ~6, ~8, and ~12 Å (Figure S18, SI). The similar porosity of Zr₆-BDC-NO₂ and Zr₆-fBDC makes them a good pair to study the impact of Lewis acidity on catalytic performance without the complication of varying diffusion kinetics through MOF channels. The number of missing linkers was determined by ¹H NMR and ICP-MS to be 0.94 per Zr₆ node, thus giving Zr₆-BDC-NO₂ the formula Zr₆(μ₃-O)₄(μ₃-OH)₄(BDC-NO₂)_{5.06}[(OH)(OH₂)]_{1.88} (Figure S16, SI). The defect density of Zr₆-BDC-NO₂ is essentially the same as that of Zr₆-fBDC.

Zr₆-BPDC-(NO₂)₂ with larger channels was synthesized in 85% yield by heating a mixture of H₂BPDC-(NO₂)₂ and ZrOCl₂·8H₂O in acidified THF at 80 °C. The H₂BPDC-(NO₂)₂ ligand was synthesized in high yield using the Pd-catalyzed Suzuki-Miyaura cross-coupling reaction followed by ester hydrolysis (Figure S4, SI). Zr₆-BPDC-(NO₂)₂ is isostructural to UiO-67 based on the

similarity of their PXRD patterns (Figure S21, SI). The porosity of The Zr₆-BPDC-(NO₂)₂ was confirmed by N₂ sorption isotherms, affording a BET surface area of 1205 m²/g and pore diameters of ~12, ~15, and ~22 Å (Figure S22, SI).

Probing Lewis acidity by superoxide EPR spectra

Spectroscopic measurements of MOFs, such as UV-vis, fluorescence and EPR measurements, have been challenging as the signals tend to be weak and noisy owing to poor dispersibility of and strong scattering by MOFs. One solution to this problem is to utilize probes that have high sensitivity toward photon excitations. We have chosen superoxide (O₂^{•-}) and N-methylacridone (NMA) as two sensitive probes to assess the Lewis acidity of MOFs. Superoxide ions display strong EPR signals and NMA is a highly emissive fluorescent dye. More importantly, their signals are sensitive to the Lewis acidity of binding metal ions. These probes were pioneered by Fukuzumi and coworkers for studying Lewis acidity of soluble metal salts.⁴⁹ In this work, we show for the first time that EPR of MOF-bound superoxide and fluorescence of MOF-bound NMA provide sensitive indicators for the Lewis acidity of MOFs.

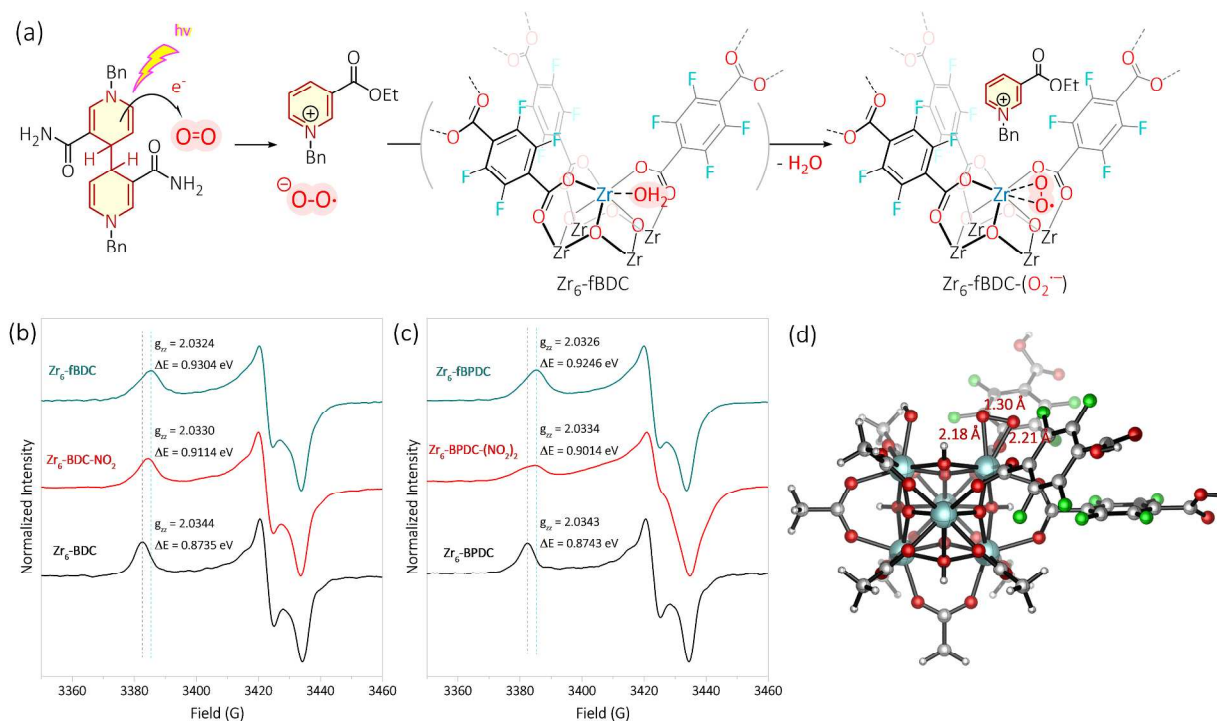


Figure 3. (a) Proposed mechanism for the superoxide binding to the defect Zr sites in Zr₆-fBDC. (b) Zr(O₂^{•-}) EPR spectra of Zr₆-BDC (black), Zr₆-BDC-NO₂ (red), and Zr₆-fBDC (blue). (c) Zr(O₂^{•-}) EPR spectra of Zr₆-BPDC (black), Zr₆-BPDC-(NO₂)₂ (red), and Zr₆-fBPDC (blue). (d) DFT optimized superoxide binding mode on Zr₆-fBDC-O₂^{•-}.

Superoxide ions (O₂^{•-}) can be generated *in situ* by the 1 e⁻ reduction of O₂ using the dimeric 1-benzyl-1,4-dihydronicotinamide [(BNA)₂] as a photoreductant. The photo-generated O₂^{•-} is very small and easily diffuses through the MOF channel before quenching. Additionally, O₂^{•-} is very electron-rich and has a strong binding affinity to Lewis acids such as the defect Zr sites in UiO-MOFs. O₂^{•-} binds to Zr active sites by displacing the weakly coordinating H₂O molecule to form the EPR-active Zr(O₂^{•-}) species (Figure 3a). Lewis acid coordination significantly changes the EPR signature of O₂^{•-}. The rhombic g-tensor of the EPR spectrum, most evidently the g_{zz} component, is diagnostic of the binding strength between O₂^{•-} and the Lewis acid.⁶² This effect is due to coordination of the electron pair in the highest doubly occupied molecular orbital (HOMO) of the O₂^{•-} π* orbitals, which increases the energy splitting (ΔE) between the HOMO and the

singly occupied molecular orbital (SOMO) of the O₂^{•-} π* orbitals. The ΔE is related to the g_{zz} value following the Känzig-Cohen equation.⁶³ Metal centers with stronger Lewis acidity should split the π* orbitals to a greater extent, thus giving larger ΔE values.

The EPR spectra of superoxide ions bound to a variety of UiO MOFs were measured on a Bruker Elexsys 500 X-band EPR spectrometer at 100 K. A clear trend was observed for the measured g_{zz} values. UiO MOFs grown from more electron-deficient dicarboxylates, namely those with electron-withdrawing groups, showed smaller g_{zz} values for the anisotropic EPR spectra, indicating larger ΔE values. Zr₆-BDC produced a g_{zz} value of 2.0344, which corresponds to a ΔE of 0.8735 eV. This ΔE is the smallest value in the UiO-66 MOF series in this study. The Zr₆-BDC-NO₂ MOF, which was previously reported to catalyze (+)-citronellal isomerization,³² showed a smaller g_{zz} value of 2.0330, which cor-

responds to a larger ΔE of 0.9114 eV. Impressively, Zr₆-fBDC exhibited a g_{zz} of 2.0324 and a ΔE of 0.9304 eV, making it the most Lewis acidic MOF in the UiO-66 series.

To validate the trend observed for the UiO-66 series, two new MOFs of UiO-67 topology were prepared. Zr₆-BPDC showed a g_{zz} of 2.0343 and a ΔE of 0.8743 eV, similar to that of Zr₆-BDC. Zr₆-BPDC-(NO₂)₂ gave a g_{zz} of 2.0334 and a ΔE of 0.9014 eV. The perfluorinated MOF, Zr₆-fBPDC, is much more Lewis acidic with a g_{zz} of 2.0326 and a ΔE of 0.9246 eV. These experiments prove that perfluorination is an effective way to enhance Lewis acidity of UiO-MOFs with defect Zr₆O₄(OH)₄ nodes.

Density Functional Theory (DFT) Calculations of Superoxide Binding on Zr Active Sites

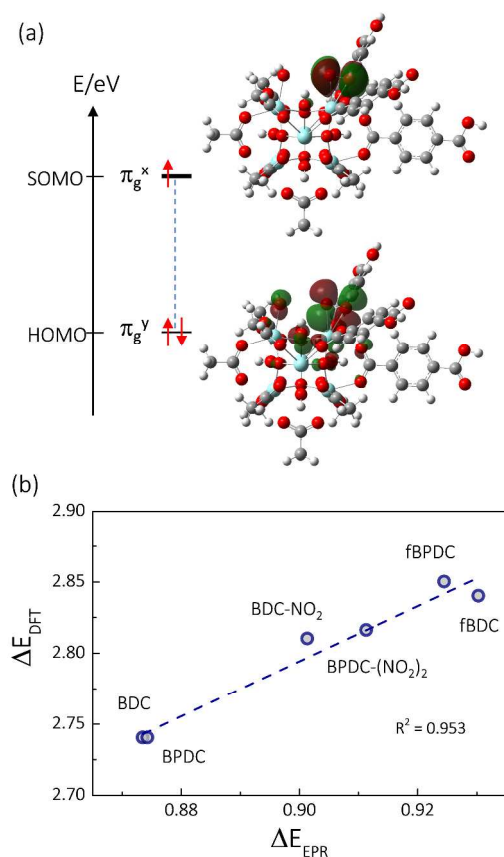


Figure 4. (a) Molecular orbital diagram for Zr(O₂^{•-}) in the model structure. The HOMO-SOMO gap for Zr₆-BDC-O₂^{•-}, indicated by the dotted line, is 2.74 eV. (b) The linear relationship between ΔE values calculated by DFT, ΔE_{DFT} , and ΔE values measured by EPR, ΔE_{EPR} , with an adjusted R^2 of 0.953.

Density functional theory (DFT) calculations were carried out to gain insight into the coordination mode and electronic structure of O₂^{•-} bound to Zr₆ nodes. To reduce the computational expense, only the three ligands that were directly connected to the Zr(O₂^{•-}) species were allowed to fully relax. The corresponding linkers and clusters were optimized at the M06 level of theory.⁶⁴ All other dicarboxylate ligands were replaced with acetates and held fixed. (Section 5.1, SI) The optimized structures for the models of all six MOFs showed a side-on binding mode of the O₂^{•-} on the Zr₆ node (Figure 3d). The side-on coordination is analogous to the one generally proposed for superoxide ions bound to a zirconia (ZrO₂) surface.⁶⁵ For the Zr₆-BDC-O₂^{•-} model structure, the O-O distance at the Zr(O₂^{•-}) site is 1.301 Å, longer than the O-O distance in a free O₂^{•-} species (1.28 Å). This is presumably due to the weakening of the O-O bond by the coordination to Zr centers. Interestingly, the Zr-O bond distances in Zr₆-BDC-(O₂^{•-}) are

2.193 and 2.231 Å, with a small degree of binding asymmetry. This effect was tentatively rationalized through electronic structure analysis of the π^* orbital, which displayed significant anti-symmetric repulsive interactions between the carboxylate electron lone pair and the superoxide π^* electrons, thus leading to the elongation of one of the Zr-O bonds (Figure S33, SI). Comparison of the Zr(O₂^{•-}) bond distances in the Zr₆-BDC and Zr₆-fBDC models offered insight into the binding strength of O₂^{•-} to different Zr centers. Indeed, the Zr-O distances in Zr₆-fBDC are 2.18 and 2.21 Å, shorter than those in Zr₆-BDC (2.19 and 2.23 Å). This computational result verified that electron withdrawing groups on the organic linker increase the Lewis acidity of Zr sites in defect UiO-MOFs, as indicated by the higher Zr(O₂^{•-}) binding strength.

The enhancement of MOF Lewis acidity by installing electron withdrawing groups on the linker was also verified by DFT through calculation of ΔE values. The molecular orbital diagram of a Zr(O₂^{•-}) fragment in the Zr₆-BDC model structure was analyzed by biorthogonalization (Figure S32). We have clearly observed that the bonding orbitals for the O₂^{•-} significantly overlap with the Zr⁴⁺ orbitals. This observation is indicative of strong binding of O₂^{•-} onto the Zr center, and not simply electrostatic attachment. The SOMO and HOMO molecular orbital eigenvalues were calculated using restricted open shell calculations (Figure 4a). The energy gap between the HOMO and SOMO is correlated to the ΔE measured from EPR analysis. We have observed that the HOMO-SOMO energy gaps increase in the following order: Zr₆-BDC \approx Zr₆-BPDC < Zr₆-BDC-NO₂ < Zr₆-BPDC-(NO₂)₂ < Zr₆-fBPDC < Zr₆-fBDC (Figure 4; Figure S34-38, SI). A linear relationship between the calculated ΔE_{DFT} with the EPR measured ΔE was observed with an adjusted R^2 of 0.953 (Figure 4b). Thus, DFT calculations support the proposal that electron-withdrawing groups on the MOF ligand significantly increase the binding strength of O₂^{•-} on the MOF node.

DFT calculations were also used to elucidate the impact of defect density on MOF Lewis acidity. For Zr₆-fBDC, two additional models for superoxide-bound MOF nodes, one with two missing carboxylates (Zr₆-fBDC-2def-O₂^{•-}) and another with three missing carboxylates (Zr₆-fBDC-3def-O₂^{•-}), were optimized and analyzed for SOMO-HOMO gaps (Section 5.3, SI). The superoxide moieties in the doubly or triply defected models adopt identical coordination modes as the singly defected model and produced identical SOMO-HOMO gaps of 2.84 eV (Figure S39-42, SI). The inclusion of more defects, unlike the exchange of carboxylates, does not alter the primary coordination environment around Lewis acidic Zr centers.

Probing Lewis acidity by NMA fluorescence

Although O₂^{•-} is an accurate indicator of MOF Lewis acidity, the experimental procedures for superoxide generation and EPR measurement are lengthy and tedious. Therefore, we have also used NMA fluorescence to probe Lewis acidity of MOFs. NMA is a commercially-available fluorescent dye, which features lone pairs that can effectively bind to vacant metal sites in MOFs. The fluorescence maxima (λ_{max}) of NMA shifts significantly upon binding to metal centers. These shifts are indicative of the binding affinity of the probe to the metals and thus can be used as a measure of Lewis acidity. A large excess of Lewis acids is typically used with respect to NMA to avoid the emission of non-coordinated NMA molecules. The fluorescence spectra of NMA coordinated to three different UiO-66 MOFs are shown in Figure 5c-d. In the case of Zr₆-BDC and Zr₆-BDC-NO₂, the λ_{max} of NMA changed dramatically from 433.0 nm to 466.4 nm and 469.0 nm, respectively, upon coordination of the dye to defect Zr sites. Zr₆-fBDC shifted the NMA emission wavelength the most, with a λ_{max} of 470.6 nm. The same trend was observed for the three UiO-67 MOFs, where the Zr₆-fBPDC shifted the NMA

emission wavelength the most, with a λ_{\max} of 469.6 nm. We also found that the λ_{\max} of Zr-bound NMA was linearly related to the ΔE measured from the EPR method, with an adjusted R-squared value of 0.954. A fitted empirical relationship (Figure 5e) between the λ_{\max} and ΔE was obtained and used to calculate the NMA fluorescence-derived ΔE values (ΔE_{NMA}) for every MOF. The ΔE_{NMA} values were compared with the EPR-measured ΔE values to check the reliability of the fluorescence method. The λ_{\max} , ΔE_{NMA} and ΔE for each of the six different MOFs are summarized in Table 1. The ΔE_{NMA} consistently reproduces the EPR-measured ΔE , indicating that the fluorescence dye is a convenient probe for assessing Lewis acidity in MOFs.

The coordination mode and electronic structure of NMA bound to the Zr₆ node was also studied by DFT. The optimized structure showed that the carbonyl group (instead of the aryl or nitrogen) is coordinated to the vacant site of the Zr₆ node, adopting a side-on coordination mode. Molecular orbital calculations of the NMA fluorescent dye revealed the electronic structure of the HOMO

orbital, which is proposed to be responsible for the NMA coordination to Zr (Figure S43, SI).

To exclude the possibility that the Brønsted acidic μ_3 -OH (pKa ~ 3.52)⁶⁶ might have caused the shift in the NMA emission, a series of Brønsted acids (trifluoroacetic acid, benzoic acid, acetic acid, and 4-aminobenzoic acid) covering the pKa range of -0.25 ~ 4.86 were mixed with NMA in MeCN to measure fluorescence. None of the four acids caused any shift in the NMA emission spectra, indicating Brønsted acids are not responsible for the shifts in NMA fluorescence in the UiO series (Figure S27, SI). For weak Lewis acids that have ΔE values less than 0.5 eV, NMA cannot coordinate to the metal centers effectively thus leading to almost no shift in emission wavelength.⁴⁹ Two common Lewis acidic MOFs, MOF-5 and HKUST-1,⁶⁷⁻⁶⁸ displayed no shift in the NMA fluorescence, indicating the Zn₄O node in MOF-5 and the Cu₂ node in HKUST-1 have ΔE values less than 0.5 eV (Figure S29, SI).

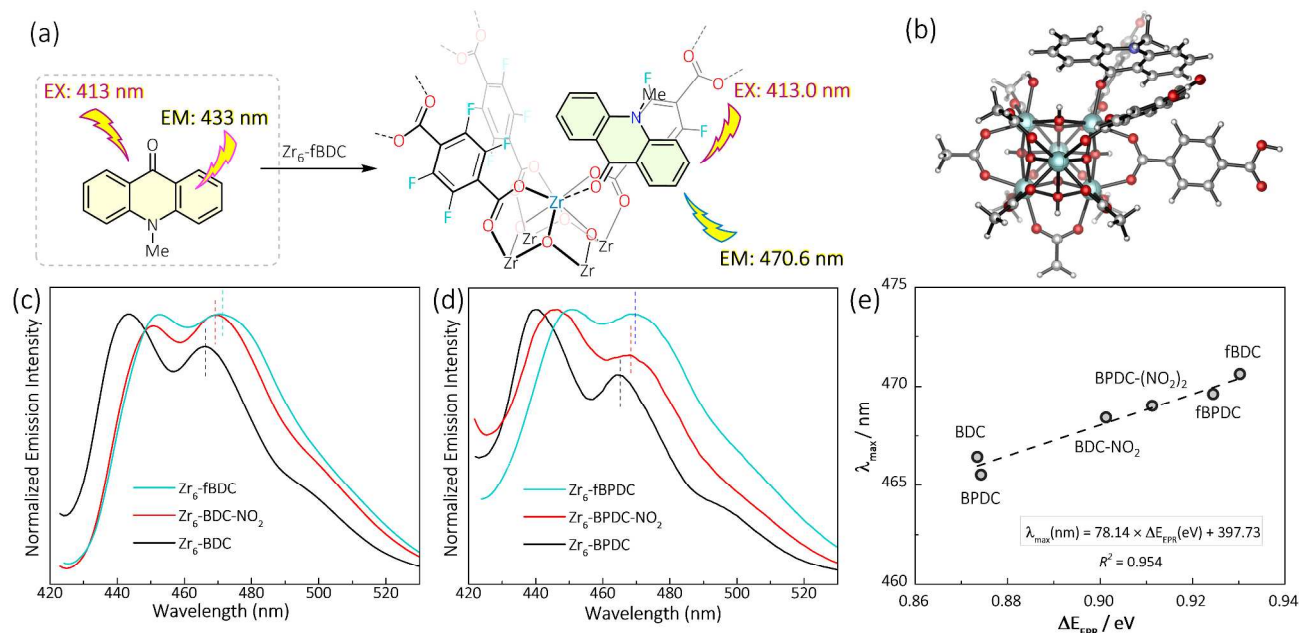


Figure 5. (a) The coordination of NMA dye to the Zr defect sites in Zr₆-fBDC, leading to a dramatic shift in the emission maxima. (b) DFT optimized coordination mode of NMA on the Zr₆ node of Zr₆-BDC. (c) Fluorescence spectra of NMA binding to Zr₆-BDC (black), Zr₆-BDC-NO₂ (red), and Zr₆-fBDC (blue) in MeCN at 298 K. (d) Fluorescence spectra of NMA binding to Zr₆-BPDC (black), Zr₆-BPDC-(NO₂)₂ (red), and Zr₆-fBPDC (blue) in MeCN at 298 K. (e) Linear relationship between the EPR measured ΔE_{EPR} and the DFT calculated ΔE_{DFT} .

Table 1. List of the fluorescence maxima (λ_{\max}), calculated ΔE_{NMA} from NMA λ_{\max} , and ΔE_{EPR} measured from Zr-(O₂^{•-}) EPR spectra.

MOFs	λ_{\max} (nm)	ΔE_{NMA} (eV)	ΔE_{EPR} (eV)
Zr ₆ -BDC	466.4	0.8788	0.8735
Zr ₆ -BDC-NO ₂	469.0	0.9121	0.9114
Zr ₆ -fBDC	470.6	0.9326	0.9304
Zr ₆ -BPDC	465.5	0.8673	0.8743
Zr ₆ -BPDC-(NO ₂) ₂	468.4	0.9044	0.9014
Zr ₆ -fBPDC	469.6	0.9200	0.9246

Perfluorinated MOF-Catalyzed Diels-Alder Reactions

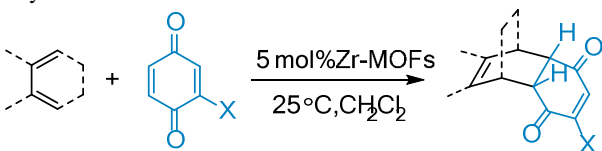
The synthesis of perfluorinated Zr-MOFs and the characterization of their prominent Lewis acidity inspired the investigation of their catalytic activities. We first tested perfluorinated Zr MOFs for Diels-Alder reactions.

The Diels-Alder reaction is of great synthetic value to the organic chemistry community and has been widely applied to the

synthesis of six-member ring structures with high regioselectivity and stereoselectivity.⁶⁹⁻⁷⁰ However, the reaction generally requires high temperatures and long reaction times when performed without the addition of an acid catalyst. Unlike classical Lewis acidic metal complexes, MOF catalysts benefit from having uniform active sites which can lead to better reaction selectivity. The solid nature of MOFs offers additional advantages, including easy separation from reaction mixtures and catalyst reusability. For the cyclization of 1,4-benzoquinone with 2,3-dimethylbuta-1,3-diene, only 4% yield of product was observed in the absence of catalyst at 25 °C after 2 h (entry 1, Table 2). In the presence of Zr₆-BDC, which has been shown to be active for ethanol dehydration at 250 °C,³⁵ the product yield increased to 14% under the same reaction conditions (entry 2, Table 2). Zr₆-BDC-NO₂, which is reported to be active for (+)-citronellal isomerization at 100 °C, increased the reaction yield to 25% at the same reaction condition (entry 3, Table 2). Under the same reaction conditions, Zr₆-fBDC afforded the cycloaddition product in 78% yield. Elongation of the reaction time from 2 h to 8 h further increased the yield to 98%. Considering Zr₆-fBDC has a higher density of defect sites, additional control experiments were performed by increasing the catalyst load-

ing of Zr₆-BDC and Zr₆-BDC-NO₂ to the same loading of defect sites as Zr₆-fBDC. However, Zr₆-fBDC still afforded the product at much higher yield than Zr₆-BDC and Zr₆-BDC-NO₂ in these experiments (Table S5, SI). The reaction is proposed to be initiated by the coordination of the lone pair electrons of the quinones to the Zr centers. This coordination is expected to lower the energy of the LUMO orbital to enhance the overlap with the HOMO orbital of the dienes. The coordination of quinones to Zr is proposed to be analogous to the coordination of NMA to Zr, since they both contain electron-rich carbonyl groups.

Table 2. Catalyst evaluation and substrate scope of Zr₆-fBDC catalyzed Diels-Alder reactions.^a



Product	Catalyst	Time	Yield
1	No catalyst	2 h	4 %
2	Zr ₆ -BDC	2 h	14 %
3	Zr ₆ -BDC-NO ₂	2 h	25 %
4	Zr ₆ -fBDC	2 h	78 %
5	Zr ₆ -fBDC	8 h	98 %
6	Zr ₆ -fBDC	12 h	94 %
7	Zr ₆ -fBDC	24 h	99 %
8	Zr ₆ -fBDC	30 h	95 %
9	Zr ₆ -fBDC	48 h	84 %
10	Zr ₆ -fBDC	48 h	74 %

^a Reaction conditions: dienophile (1 equiv., 1 mmol), diene (1.2 equiv.), Zr MOFs (5 mol%, 0.05 mmol), CH₂Cl₂ (3.0 mL), 25 °C. Reaction yields were determined from ¹H NMR using mesitylene as an internal standard.

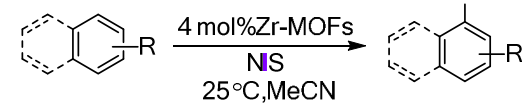
The MOF-catalyzed Diels-Alder reaction displayed a broad substrate scope (entry 5-10, Table 2). Cyclohexa-1,3-diene, a less reactive diene than cyclopentadiene or 2,3-dimethylbuta-1,3-diene, was cyclized with 1,4-benzoquinone in 94% yield in 12h in the presence of 5 mol% Zr₆-fBDC.⁷¹ Quinone substrates containing electron-donating groups, such as the 2-methyl-1,4-benzoquinone, are generally less reactive in Diels-Alder reactions due to their much higher LUMO energy. The presence of a methyl group also greatly increases the steric hindrance of the quinone substrate. Impressively, in the presence of 5 mol% Zr₆-fBDC, 2-methyl-1,4-benzoquinone efficiently reacted with cyclo-

hexa-1,3-diene and 2,3-dimethylbuta-1,3-diene at 25 °C to afford cycloaddition products in 74% and 84% yields, respectively. Moreover, Zr₆-fBDC was reused for at least three runs without significant loss of catalytic activity for the cyclization of 2,3-dimethylbuta-1,3-diene with 2-chloro-1,4-benzoquinone (Figure S44, SI).

Perfluorinated MOF-Catalyzed Arene C-H Iodination Reactions

Aryl iodides are very useful building blocks in organic synthesis. The C-I bonds of arenes readily undergo cross-coupling reactions and nucleophilic substitutions.⁷²⁻⁷³ There are multiple synthetic methods to access these compounds, including the Sandmeyer reaction, halide exchange reactions, and electrophilic substitutions. The most straightforward method is the direct C-H iodination using iodine or N-iodosuccinimide (NIS).⁷⁴⁻⁷⁵ Many acid catalysts have been developed to perform such reactions, notably the BF₃-H₂O system reported by Olah and co-workers which could iodinate very challenging electron-deficient arenes.⁷⁶ For electron-rich arenes, however, many catalysts suffer from poor regioselectivity, leading to the formation of multi-iodinated products.⁷⁷ Zr₆-fBDC was tested for the iodination of anisole at 25 °C using MeCN as the solvent. These conditions afforded exclusively the mono-iodination product in 96% yield after 30 h. Other arene substrates, such as 2-methoxynaphthalene, aniline, and N-methylaniline, were also iodinated in high yields with excellent regioselectivity (entry 5-8, Table 3).

Table 3. Catalyst evaluation and substrate scope of Zr₆-fBDC catalyzed C-H iodination reactions.^a



Product	Catalyst	Time	Yield
1	No catalyst	12 h	10 %
2	Zr ₆ -BDC	12 h	16 %
3	Zr ₆ -BDC-NO ₂	12 h	28 %
4	Zr ₆ -fBDC	12 h	85 %
5	Zr ₆ -fBDC	18 h	81 %
6	Zr ₆ -fBDC	30 h	96 %
7	Zr ₆ -fBDC	2 h	95 %
8	Zr ₆ -fBDC	2 h	93 %

^a Reaction conditions: arenes (1 equiv., 0.5 mmol), N-iodosuccinimide (1.1 equiv.), Zr MOFs (4 mol%, 0.02 mmol), MeCN (1.5 mL), 25 °C. Reaction yields were determined from ¹H NMR using mesitylene as an internal standard.

The catalytic performance of Zr₆-fBDC was compared to other MOFs to show the importance of ligand perfluorination. At identical reaction conditions and catalyst loading, Zr₆-BDC and Zr₆-BDC-NO₂ only iodinated 2-methoxynaphthalene in 16% and 28% yield, respectively, while Zr₆-fBDC gave 85% yield of the 3-iodinated product. Even when the catalyst loadings of Zr₆-BDC and Zr₆-BDC-NO₂ were increased to the same loading of defect

1 sites as Zr₆-fBDC, the yields of product were still much lower
2 than that of Zr₆-fBDC (Table S6, SI). Other Lewis acidic MOF
3 catalysts, e.g., MOF-5 and HKUST-1, also displayed much lower
4 catalytic performance than Zr₆-fBDC (Table S8). Impressively,
5 Zr₆-fBDC could be recycled at least 6 times without a significant
6 drop in catalytic activity, illustrating the robustness of the solid
7 Lewis acid catalyst (Figure S47, SI).

8 CONCLUSION

9 We developed two general methods for quantifying the Lewis
10 acidity of MOFs by measuring the changes in superoxide EPR
11 signals and shifts of NMA fluorescence peaks upon their coordi-
12 nation to MOFs. We prepared a series of UiO-MOFs featuring
13 defect Zr₆O₄(OH)₄ nodes with missing linkers and unsaturated
14 coordination around Zr active sites. The application of the EPR
15 and fluorescence methods to a variety of MOFs unveiled a strong
16 correlation between dicarboxylate electron density and
17 Zr₆O₄(OH)₄ Lewis acidity, leading to the discovery of signifi-
18 cantly enhanced Lewis acidity within Zr-MOFs containing perfluori-
19 nated bridging ligands. The new perfluorinated MOFs, Zr₆-fBDC
20 and Zr₆-fBPDC, are significantly more Lewis acidic than non-
21 substituted UiO-66 and UiO-67 as well as the nitrated MOFs Zr₆-
22 BDC-NO₂ and Zr₆-BPDC-(NO₂)₂. Zr₆-fBDC was shown to be a
23 highly active Lewis acid catalyst for Diels-Alder and arene C-H
24 iodination reactions. This work, thus, establishes the important
25 role of ligand perfluorination in enhancing MOF Lewis acidity
26 and the potential of designing new, highly Lewis acidic MOFs as
27 single-site porous solid catalysts for fine chemical synthesis.

28 ASSOCIATED CONTENT

29 Supporting Information

30 This material is available free of charge via the Internet at
31 <http://pubs.acs.org>. Synthesis and characterization of the ligands
32 and MOFs; procedures for DFT calculations; procedures for the
33 superoxide binding and fluorescent dye binding; procedures for the
34 Diels-Alder reactions and regioselective C-H iodination reac-
35 tions. Crystallographic data for Me₂fBPDC (CCDC 1845893).

36 AUTHOR INFORMATION

37 Corresponding Author

38 wenbinlin@uchicago.edu

39 Author Contribution

40 P. J. and T. D. contributed equally.

41 Notes

42 The authors declare no competing financial interest.

43 ACKNOWLEDGMENT

44 We thank Prof. John Anderson and Dr. Ethan Hill for help with
45 EPR measurements. This work was supported by NSF (CHE-
46 1464941). XAS analysis was performed at Beamline 10-BM. Use
47 of the Advanced Photon Source, an Office of Science User Facili-
48 ty operated for the U.S. DOE Office of Science by ANL, was
49 supported by the U.S. DOE under Contract No. DE-AC02-
50 06CH11357.

51 References

52 1. Ma, L.; Abney, C.; Lin, W., *Chem. Soc. Rev.* **2009**, *38*, 1248-
53 1256.

2. Lee, J.; Farha, O. K.; Roberts, J.; Scheidt, K. A.; Nguyen, S. T.; Hupp, J. T., *Chem. Soc. Rev.* **2009**, *38*, 1450-1459.
3. Ingleson, M. J.; Barrio, J. P.; Bacsá, J.; Dickinson, C.; Park, H.; Rosseinsky, M. J., *Chem. Commun.* **2008**, 1287-1289.
4. Wang, Z.; Cohen, S. M., *Chem. Soc. Rev.* **2009**, *38*, 1315-1329.
5. Uemura, T.; Yanai, N.; Kitagawa, S., *Chem. Soc. Rev.* **2009**, *38*, 1228-1236.
6. Liu, Y.; Xuan, W.; Cui, Y., *Adv. Mater.* **2010**, *22*, 4112-4135.
7. Alexandra, F.; A., C. P.; P., I. C.; A., T. A.; Z., K. Y.; V., W. P.; R., D. J.; J., R. M., *Angew. Chem.* **2012**, *124*, 7558-7562.
8. Yoon, M.; Srirambalaji, R.; Kim, K., *Chem. Rev.* **2012**, *112*, 1196-1231.
9. Gu, Z. Y.; Park, J.; Raiff, A.; Wei, Z.; Zhou, H. C., *ChemCatChem* **2014**, *6*, 67-75.
10. Liu, J.; Chen, L.; Cui, H.; Zhang, J.; Zhang, L.; Su, C.-Y., *Chem. Soc. Rev.* **2014**, *43*, 6011-6061.
11. Zhao, M.; Ou, S.; Wu, C.-D., *Acc. Chem. Res.* **2014**, *47*, 1199-1207.
12. Jiang, J.; Gándara, F.; Zhang, Y.-B.; Na, K.; Yaghi, O. M.; Klemperer, W. G., *J. Am. Chem. Soc.* **2014**, *136*, 12844-12847.
13. Choi, K. M.; Na, K.; Somorjai, G. A.; Yaghi, O. M., *J. Am. Chem. Soc.* **2015**, *137*, 7810-7816.
14. Chen, Y. Z.; Wang, C.; Wu, Z. Y.; Xiong, Y.; Qiang, X.; Yu, S. H.; Jiang, H. L., *Adv. Mater.* **2015**, *27*, 5010-5016.
15. Xiao, D. J.; Oktawiec, J.; Milner, P. J.; Long, J. R., *J. Am. Chem. Soc.* **2016**, *138*, 14371-14379.
16. Metzger, E. D.; Comito, R. J.; Hendon, C. H.; Dincă, M., *J. Am. Chem. Soc.* **2017**, *139*, 757-762.
17. Zhang, T.; Manna, K.; Lin, W., *J. Am. Chem. Soc.* **2016**, *138*, 3241-3249.
18. Manna, K.; Ji, P.; Lin, Z.; Greene, F. X.; Urban, A.; Thacker, N. C.; Lin, W., *Nat. Commun.* **2016**, *7*, 12610.
19. Noh, H.; Cui, Y.; Peters, A. W.; Pahls, D. R.; Ortuño, M. A.; Vermeulen, N. A.; Cramer, C. J.; Gagliardi, L.; Hupp, J. T.; Farha, O. K., *J. Am. Chem. Soc.* **2016**, *138*, 14720-14726.
20. Na, K.; Choi, K. M.; Yaghi, O. M.; Somorjai, G. A., *Nano Lett.* **2014**, *14*, 5979-5983.
21. An, B.; Zhang, J.; Cheng, K.; Ji, P.; Wang, C.; Lin, W., *J. Am. Chem. Soc.* **2017**, *139*, 3834-3840.
22. Lian, X.; Fang, Y.; Joseph, E.; Wang, Q.; Li, J.; Banerjee, S.; Lollar, C.; Wang, X.; Zhou, H.-C., *Chem. Soc. Rev.* **2017**, *46*, 3386-3401.
23. Zhang, Z.-M.; Zhang, T.; Wang, C.; Lin, Z.; Long, L.-S.; Lin, W., *J. Am. Chem. Soc.* **2015**, *137*, 3197-3200.
24. Fortea-Pérez, F. R.; Mon, M.; Ferrando-Soria, J.; Boronat, M.; Leyva-Pérez, A.; Corma, A.; Herrera, J. M.; Osadchii, D.; Gascon, J.; Armentano, D.; Pardo, E., *Nat. Mater.* **2017**, *16*, 760.
25. Phan, A.; Czaja, A. U.; Gándara, F.; Knobler, C. B.; Yaghi, O. M., *Inorg. Chem.* **2011**, *50*, 7388-7390.
26. Xiao, D. J.; Bloch, E. D.; Mason, J. A.; Queen, W. L.; Hudson, M. R.; Planas, N.; Borycz, J.; Dzubak, A. L.; Verma, P.; Lee, K.; Bonino, F.; Crocellà, V.; Yano, J.; Bordiga, S.; Truhlar, D. G.; Gagliardi, L.; Brown, C. M.; Long, J. R., *Nat. Chem.* **2014**, *6*, 590.
27. Ji, P.; Solomon, J. B.; Lin, Z.; Johnson, A.; Jordan, R. F.; Lin, W., *J. Am. Chem. Soc.* **2017**, *139*, 11325-11328.
28. Fujita, M.; Kwon, Y. J.; Washizu, S.; Ogura, K., *J. Am. Chem. Soc.* **1994**, *116*, 1151-1152.
29. Evans, O. R.; Ngo, H. L.; Lin, W., *J. Am. Chem. Soc.* **2001**, *123*, 10395-10396.
30. Bai, Y.; Dou, Y.; Xie, L.-H.; Rutledge, W.; Li, J.-R.; Zhou, H.-C., *Chem. Soc. Rev.* **2016**, *45*, 2327-2367.
31. Yuan, S.; Qin, J.-S.; Lollar, C. T.; Zhou, H.-C., *ACS Central Science* **2018**, *4*, 440-450.
32. Vermoortele, F.; Vandichel, M.; Voorde, B. V. d.; Ameloot, R.; Waroquier, M.; Speybroeck, V. V.; Vos, D. E. D., *Angew. Chem. Int. Ed.* **2012**, *51*, 4887-4890.

33. Vermoortele, F.; Bueken, B.; Le Bars, G.; Van de Voorde, B.; Vandichel, M.; Houthoofd, K.; Vimont, A.; Daturi, M.; Waroquier, M.; Van Speybroeck, V.; Kirschhock, C.; De Vos, D. E., *J. Am. Chem. Soc.* **2013**, *135*, 11465-11468.
34. Mondloch, J. E.; Katz, M. J.; Isley III, W. C.; Ghosh, P.; Liao, P.; Bury, W.; Wagner, G. W.; Hall, M. G.; DeCoste, J. B.; Peterson, G. W.; Snurr, R. Q.; Cramer, C. J.; Hupp, J. T.; Farha, O. K., *Nat. Mater* **2015**, *14*, 512.
35. Yang, D.; Ortuño, M. A.; Bernales, V.; Cramer, C. J.; Gagliardi, L.; Gates, B. C., *J. Am. Chem. Soc.* **2018**, *140*, 3751-3759.
36. Beyzavi, M. H.; Klet, R. C.; Tussupbayev, S.; Borycz, J.; Vermeulen, N. A.; Cramer, C. J.; Stoddart, J. F.; Hupp, J. T.; Farha, O. K., *J. Am. Chem. Soc.* **2014**, *136*, 15861-15864.
37. Rasero-Almansa, A. M.; Iglesias, M.; Sanchez, F., *RSC Adv.* **2016**, *6*, 106790-106797.
38. Sang, X.; Zhang, J.; Xiang, J.; Cui, J.; Zheng, L.; Zhang, J.; Wu, Z.; Li, Z.; Mo, G.; Xu, Y.; Song, J.; Liu, C.; Tan, X.; Luo, T.; Zhang, B.; Han, B., *Nat. Commun.* **2017**, *8*, 175.
39. Ly, H. G. T.; Fu, G.; Kondinski, A.; Bueken, B.; De Vos, D.; Parac-Vogt, T. N., *J. Am. Chem. Soc.* **2018**, *140*, 6325-6335.
40. Zou, R.-Q.; Sakurai, H.; Han, S.; Zhong, R.-Q.; Xu, Q., *J. Am. Chem. Soc.* **2007**, *129*, 8402-8403.
41. Horike, S.; Dincă, M.; Tamaki, K.; Long, J. R., *J. Am. Chem. Soc.* **2008**, *130*, 5854-5855.
42. Henschel, A.; Gedrich, K.; Kraehnert, R.; Kaskel, S., *Chem. Commun.* **2008**, 4192-4194.
43. Shultz, A. M.; Farha, O. K.; Hupp, J. T.; Nguyen, S. T., *J. Am. Chem. Soc.* **2009**, *131*, 4204-4205.
44. Tanabe, K. K.; Cohen, S. M., *Inorg. Chem.* **2010**, *49*, 6766-6774.
45. Srirambalaji, R.; Hong, S.; Natarajan, R.; Yoon, M.; Hota, R.; Kim, Y.; Ho Ko, Y.; Kim, K., *Chem. Commun.* **2012**, *48*, 11650-11652.
46. Jiang, Z. R.; Wang, H.; Hu, Y.; Lu, J.; Jiang, H. L., *Chemsuschem* **2015**, *8*, 878-885.
47. Alaerts, L.; Séguin, E.; Poelman, H.; Thibault - Starzyk, F.; Jacobs, P. A.; De Vos, D. E., *Chem. Eur. J* **2006**, *12*, 7353-7363.
48. Horcajada, P.; Surble, S.; Serre, C.; Hong, D.-Y.; Seo, Y.-K.; Chang, J.-S.; Grenèche, J.-M.; Margiolaki, I.; Ferey, G., *Chem. Commun.* **2007**, 2820-2822.
49. Ohkubo, K.; Menon, S. C.; Orita, A.; Otera, J.; Fukuzumi, S., *J. Org. Chem.* **2003**, *68*, 4720-4726.
50. Katz, M. J.; Brown, Z. J.; Colon, Y. J.; Siu, P. W.; Scheidt, K. A.; Snurr, R. Q.; Hupp, J. T.; Farha, O. K., *Chem. Commun.* **2013**, *49*, 9449-9451.
51. Wu, H.; Chua, Y. S.; Krungleviciute, V.; Tyagi, M.; Chen, P.; Yildirim, T.; Zhou, W., *J. Am. Chem. Soc.* **2013**, *135*, 10525-10532.
52. Shearer, G. C.; Chavan, S.; Ethiraj, J.; Vitillo, J. G.; Svelle, S.; Olsbye, U.; Lambert, C.; Bordiga, S.; Lillerud, K. P., *Chem. Mater.* **2014**, *26*, 4068-4071.
53. A., T. C.; J., G. K.; Seungkyu, L.; Felipe, G.; Hans - Beat, B.; M., Y. O., *Angew. Chem. Int. Ed.* **2015**, *54*, 11162-11167.
54. Cai, G.; Jiang, H. L., *Angew. Chem. Int. Ed.* **2017**, *56*, 563-567.
55. Stefano, D.; Konstantin, E.; R., H. W.; Gregor, K.; A., F. R., *Adv. Mater.* **2018**, 1704501.
56. Yang, C.; Wang, X.; Omary, M. A., *J. Am. Chem. Soc.* **2007**, *129*, 15454-15455.
57. Yang, C.; Wang, X.; Omary, M. A., *Angew. Chem. Int. Ed.* **2009**, *48*, 2500-2505.
58. Chen, T.-H.; Popov, I.; Zenasni, O.; Daugulis, O.; Miljanic, O. S., *Chem. Commun.* **2013**, *49*, 6846-6848.
59. Noro, S.-i.; Nakamura, T., *Npg Asia Materials* **2017**, *9*, e433.
60. Cheplakova, A. M.; Kovalenko, K. A.; Samsonenko, D. G.; Lazarenko, V. A.; Khrustalev, V. N.; Vinogradov, A. S.; Karpov, V. M.; Platonov, V. E.; Fedin, V. P., *Dalton Trans.* **2018**, *47*, 3283-3297.
61. Yang, D.; Odoh, S. O.; Borycz, J.; Wang, T. C.; Farha, O. K.; Hupp, J. T.; Cramer, C. J.; Gagliardi, L.; Gates, B. C., *ACS Catal.* **2016**, *6*, 235-247.
62. Sobańska, K.; Krasowska, A.; Mazur, T.; Podolska-Serafin, K.; Pietrzyk, P.; Sojka, Z., *Top. Catal.* **2015**, *58*, 796-810.
63. Känzig, W.; Cohen, M. H., *Phys. Rev. Lett.* **1959**, *3*, 509-510.
64. Zhao, Y.; Truhlar, D. G., *Theor. Chem. Acc.* **2008**, *120*, 215-241.
65. Bedilo, A. F.; Plotnikov, M. A.; Mezentseva, N. V.; Volodin, A. M.; Zhidomirov, G. M.; Rybkin, I. M.; Klabunde, K. J., *PCCP* **2005**, *7*, 3059-3069.
66. Islamoglu, T.; Atilgan, A.; Moon, S.-Y.; Peterson, G. W.; DeCoste, J. B.; Hall, M.; Hupp, J. T.; Farha, O. K., *Chem. Mater.* **2017**, *29*, 2672-2675.
67. Vishnyakov, A.; Ravikovitch, P. I.; Neimark, A. V.; Bülow, M.; Wang, Q. M., *Nano Lett.* **2003**, *3*, 713-718.
68. Kaye, S. S.; Dailly, A.; Yaghi, O. M.; Long, J. R., *J. Am. Chem. Soc.* **2007**, *129*, 14176-14177.
69. Nicolaou, K. C.; Snyder, S. A.; Montagnon, T.; Vassilikogiannakis, G., *Angew. Chem. Int. Ed.* **2002**, *41*, 1668-1698.
70. Woodward, R. B.; Sondheimer, F.; Taub, D.; Heusler, K.; McLamore, W. M., *J. Am. Chem. Soc.* **1952**, *74*, 4223-4251.
71. Ahrendt, K. A.; Borths, C. J.; MacMillan, D. W. C., *J. Am. Chem. Soc.* **2000**, *122*, 4243-4244.
72. Ma, D.; Cai, Q., *Acc. Chem. Res.* **2008**, *41*, 1450-1460.
73. Kambe, N.; Iwasaki, T.; Terao, J., *Chem. Soc. Rev.* **2011**, *40*, 4937-4947.
74. Racys, D. T.; Sharif, S. A. I.; Pimlott, S. L.; Sutherland, A., *J. Org. Chem.* **2016**, *81*, 772-780.
75. Wu, J.; He, D.; Zhang, L.; Liu, Y.; Mo, X.; Lin, J.; Zhang, H., *Org. Lett.* **2017**, *19*, 5438-5441.
76. Prakash, G. K. S.; Mathew, T.; Hoole, D.; Esteves, P. M.; Wang, Q.; Rasul, G.; Olah, G. A., *J. Am. Chem. Soc.* **2004**, *126*, 15770-15776.
77. Racys, D. T.; Warrilow, C. E.; Pimlott, S. L.; Sutherland, A., *Org. Lett.* **2015**, *17*, 4782-4785.

For Table of Contents Only

